Development of a framework for automatic quantification of uncertainty in seismic cone penetration testing

Timo Zheng[1#], *Róisín* Buckley[1], and *Eky* Febrianto[1]

[1]*James Watt School of Engineering, University of Glasgow, Glasgow, UK*
[#]*Email: t.zheng.1@research.gla.ac.uk*

ABSTRACT

Accurate quantification of the shear wave velocity, V_s, of geo-materials is an important consideration in geotechnical design. Seismic Cone Penetration Testing (SCPT) measures shear wave travel times from a source to in situ receivers along assumed travel paths to calculate V_s. Despite complexities and uncertainties associated with obtaining V_s, results are often reported to designers as a single deterministic profile without an intuitive measure of uncertainty that can be incorporated into the design process. A rigorous workflow to rapidly obtain uncertainty-quantified profiles from SCPT using a Bayesian inversion approach is developed. While similar approaches have been documented, this inversion approach explicitly considers sources of measurement error which are generally neglected (i.e., assumed to be low) in order to deliver more realistic probability distributions of true V_s and improve robustness against imperfect data. Such errors can remain undetected when using traditional approaches, despite potentially leading to inaccuracy. Additionally, an outlier detection framework is incorporated into the workflow to improve accuracy. The workflow is demonstrated by application to a large database of SCPT data. The results show significant improvement over existing methods in terms of robustness and validity, and therefore that the workflow is a valuable tool for practical analyses. Further, they provide crucial insight into the prevalence and magnitude of key errors which are traditionally present but undetected.

Keywords: Seismic; SCPT; Uncertainty quantification; Bayesian approach.

1. Introduction

Accurate estimation of the shear wave velocity, V_s, of soils and rocks is an important consideration in several geotechnical design applications. The small-strain shear modulus, G_{max}, is calculated from V_s and the density of the soil, ρ, using elastic theory,

$$G_{max} = \rho V_s^2 \quad . (1)$$

Offshore wind-turbine foundation designers, in particular, require reliable profiles of G_{max}: (i) for input into soil-structure interaction models to calculate resonant frequencies of the foundation-turbine system, and (ii) as one of several critical inputs into 1D or 3D finite element models used for limit state analysis.

While V_s can be estimated in the laboratory using bender element or resonant column tests, the results are strongly influenced by sample disturbance, confining stress, and initial void ratio. In situ tests often give more representative results (e.g., Vinck 2021). V_s profiles can be obtained in the field using a range of in situ techniques, such as Crosshole/Downhole Seismic or Seismic Cone Penetration Testing (SCPT), the latter of which represents the focus of this paper. SCPT measures travel times for shear waves from a source on the surface to below ground receivers, along assumed travel paths, to calculate V_s. Despite the complexities and uncertainties associated with this process, and the fact that any errors in V_s are amplified in the calculation of G_{max}, results are often reported to designers as a single deterministic dataset without an intuitive measure of uncertainty that can be incorporated in the design process.

This paper outlines a robust workflow to rapidly obtain uncertainty-quantified profiles of V_s from dual receiver SCPT via a Bayesian inversion approach. An existing maximum likelihood approach (see Tarantola 2005 and Pidlisecky and Haines 2011), which considers only one source of uncertainty, is extended. In the new workflow, additional errors encountered in real, imperfect datasets are dealt with explicitly and reflected in the results. It can therefore be applied within industry, providing valid, meaningful results which depict the level of uncertainty directly. Firstly, literature on SCPT interpretation is reviewed, before the Pidlisecky and Haines (2011) (PH) method is applied to a large, publicly available dataset. The results are then interrogated, and the updated method is developed and demonstrated.

2. Seismic Cone Penetration Testing

2.1. Acquisition

The focus of this paper is on SCPTs; however, the same methodology can also be applied to Downhole Seismic Testing data. The SCPT was first developed by Campanella et al. (1986) for offshore applications: the set-up consisted of a seismic receiver contained in a standard CPT that is pushed into the soil and stopped at pre-determined intervals to measure waves generated at the surface. The most widely used configuration is shown in Figure 1.

A shear wave source is located on the surface and used to generate a seismic wave that is recorded by sensors incorporated within the CPT module. Shear waves are measured by one or two sensor packages

within the module that include three orthogonally-placed receivers (two in the horizontal directions, *X* and *Y*, and one in the vertical direction, *Z*). Where dual receiver packages are used, they are typically located a fixed distance of 0.5 m apart. Repeat signals (known as *shots*) are acquired at each test location to facilitate signal stacking and stored using a seismograph.

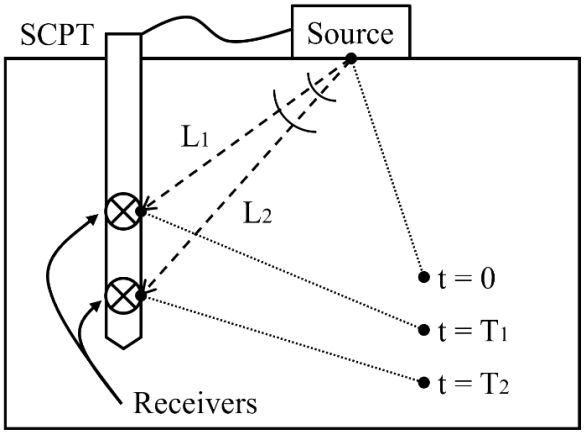

Figure 1. Typical SCPT configuration.

2.2. Interpretation

The shear wave velocity is typically calculated for each pair of successive receiver positions; *true-interval* (TI) testing acquires simultaneous measurements in a dual-receiver set-up, while *pseudo-interval* (PI) testing acquires asynchronous measurements from a single receiver at consecutive depths. In both cases, a method is required to calculate both the travel time difference, ΔT, and the travel path length ΔL such that (see Figure 1):

$$V_s = \frac{L_2 - L_1}{T_2 - T_1} = \frac{\Delta L}{\Delta T} \quad . (2)$$

Interpretation of V_s from SCPT testing is non-trivial. Travel time and ray path estimation can be carried out using a range of methods of varying complexity, reliability, and subjectivity; e.g. Stolte and Cox (2019).

Judgement-based methods to calculate ΔT – such as comparing characteristic points on the signals from each receiver – can give consistent results where the analyst has significant experience. Stolte and Cox (2019), however, posed that they can lead to subjective results for non-standard datasets and resist automation. The implementation of the cross-correlation (CC) function, $\varphi_{xy}(t)$, between the two signals has therefore become a popular method for travel time estimation (Baziw 1993):

$$\varphi_{xy}(t) = \sum_k X_k Y_{k+t} \quad , (3)$$

where X_k is the data from signal *X* at time step *k*, *t* is the induced time shift between the two signals, and Y_{k+t} is the data from signal *Y* at time step $k+t$. The time shift at the maximum cross correlation value is equal to the relative travel time between the two signals. This method is often preferred over analysis using characteristic points due to its reduced subjectivity and ease of automation.

The travel path length can be estimated either by: (i) assuming the ray follows a straight line from source to receiver, or (ii) accounting for refraction of the ray path in different velocity layers using Snell's law in a ray tracing (RT) algorithm (e.g., Wang et al. 2021). The latter will lead to more accurate results at shallower depths, where larger source offsets are used and in highly stratified profiles with varying stiffness and therefore V_s.

2.3. Uncertainty

Parasie et al. (2022) provide a systematic review of uncertainties dominant in SCPT testing in over-consolidated clays and dense sands that includes those related to instrumentation, data acquisition, and interpretation. Accurate ray path estimation and the influence of noise rank high on their list of uncertainties. Therefore, interpretation can be particularly challenging in heterogeneous profiles or noisy environments. Other key uncertainties relate to geometric concerns (e.g., source offset and depth inaccuracies – see Peuchen and Wemmenhove 2020 for further discussion on depth), signal characteristics, and timing errors. The latter are assumed to be small, and it is suggested that their magnitude is linked to the sampling rate. In absence of an agreed method to classify and quantify the uncertainty inherent in the estimation of V_s, analysts must use their judgement and experience in a somewhat arbitrary process to assess the quality of the data and interpretation and how or whether to report the final value.

One such process uses the maximum value of a normalized version of the CC function (known as the CC coefficient) – which ranges between 0 for non-correlated signals to 1 for fully correlated signals – to indicate reliability. However, this has been shown to be an unreliable indicator since measurement noise can also be correlated (Baziw and Verbeek 2016). The latter Authors incorporated CC as part of a wider data quality classification framework that considers other signal characteristics to classify the data quality.

Bayesian analysis is emerging as a useful tool for quantitative uncertainty consideration within geotechnics (e.g., Buckley et al. 2023, Stuyts et al. 2022, Lo et al. 2021). Pidlisecky and Haines (2011), following Malinverno and Briggs (2004) and Tarantola (2005), employ a Bayesian approach to quantify maximum likelihood probability distributions of V_s in single-receiver downhole seismic testing. The approach allows uncertainty in shear wave arrival time to be propagated through to derived V_s values, leading to easily interpretable probability distributions of V_s, from which low, mean, and high estimates can be extracted. Pidlisecky and Haines (2011) considered single-receiver SCPT testing in a relatively homogenous sand profile and used RT to deal with curved ray paths.

3. Existing Bayesian inversion approach

3.1. Review of existing method

This section provides a brief overview of the PH method, which utilises Bayesian inversion through maximum likelihood estimates (MLE). For a full description of the method, see Pidlisecky and Haines (2011) and Tarantola (2005). The full dataset for a given location comprises several signal traces (each corresponding to a shot) for each receiver depth. The method notes that every

possible combination of receiver depths is associated with a relative travel time, which acts as an *observation* containing information on the V_s profile. Further, these observations can be defined as uncertain to facilitate a probabilistic framework. Thus, the method begins by listing every possible pair of receiver depths, and for each pair, using the CC method to evaluate the travel times for every possible combination of signal traces (i.e., if 10 shots are available for each depth, 100 travel times will be calculated for the pair). Then, for the given pair, the observation is defined via a mean and variance, evaluated from the sample set of travel times (capturing natural variance/uncertainty in arrival time). This results in a large number of travel time observations, represented by a mean travel time vector $\boldsymbol{t}$ containing all observations, and, a covariance matrix $\mathbf{C_d}$ containing the corresponding variances along the diagonal.

It is then noted that the travel time observations are related to the reciprocal of V_s, i.e., the slowness s, and the ray paths along which the signals travel. If the s profile is discretised into increments between each receiver depth, the following matrix relationship can be defined:

$$\boldsymbol{t} = \mathbf{G}\boldsymbol{s} \quad . (4)$$

To build the matrix $\mathbf{G}$ for a given row containing travel time $t_{mn} = T_n - T_m$, the piecewise ray paths from source to depths d_n and d_m are derived, where each piece is linear within the layers between receiver depths. Then, the j^{th} term within the row is equal to the ray length for the j^{th} layer of the d_n path subtract the ray length for the j^{th} layer of the d_m path. From here, Tarantola (2005) shows that the most likely $\boldsymbol{s}$ as well as the corresponding covariance matrix $\mathbf{C_s}$ can be estimated:

$$\boldsymbol{s_{MLE}} = \left(\mathbf{G}^{\mathrm{T}}\mathbf{C_d}^{-1}\boldsymbol{G}\right)^{-1}\left(\mathbf{G}^{\mathrm{T}}\mathbf{C_d}^{-1}\boldsymbol{t} + \mathbf{C_p}^{-1}\boldsymbol{s_p}\right) \quad , (5)$$

$$\mathbf{C_s} = \left(\mathbf{G}^{\mathrm{T}}\mathbf{C_d}^{-1}\boldsymbol{G} + \mathbf{C_p}^{-1}\right)^{-1} \quad , (6)$$

where $\boldsymbol{s_p}$ and $\mathbf{C_p}$ contain prior estimations of $\boldsymbol{s}$ and $\mathbf{C_s}$ (these terms are ignored in the original method, i.e., no prior knowledge). Finally, the slowness of each layer i can be modelled as a normal distribution with mean equal to the i^{th} value of $\boldsymbol{s_{MLE}}$ and variance given by the i^{th} value along the diagonal of $\mathbf{C_s}$.

Note that in order to build $\mathbf{G}$, a RT model is used which itself depends on the slowness vector $\boldsymbol{s}$. Therefore, this problem must be solved iteratively, first assuming a constant $\boldsymbol{s}$ to build the $\mathbf{G}$ matrix, then evaluating the output $\boldsymbol{s_{MLE}}$, and subsequently updating $\mathbf{G}$ via the ray tracing model until convergence in $\boldsymbol{s_{MLE}}$ is achieved.

In addition to the above, several refinements/ additions were made as described in Table 1.

Table 1. Refinements during implementation.

Feature	Description
Filtering	All signal traces were pre-processed using a 100 Hz low-pass filter.
***X*/*Y*/*Z* selection**	For each location, the full set of *X* components or the full set of *Y* components were considered depending on which exhibited greater average signal power.
Inversion	Due to a lack of receiver at the surface, the $\mathbf{G}$ matrix is poorly conditioned to solve for the slowness between the surface and the uppermost receiver. Therefore, this value is assumed equal to the slowness of the subsequent layer.
Iteration	The inversion was iterated until 95% of slowness values experienced a <1% change, up to a maximum of 20 iterations.

3.2. Test data

The method outlined in the previous section was implemented and tested across a range of 110 SCPT locations acquired across four sites within the Dutch Offshore Wind sector. These data are owned and made publicly accessible by RVO.

Only seabed mode SCPTs were considered, which generally comprise tests at 0.5–1.0 m depth increments. At each test depth, 4–10 non-polarised shot repetitions were performed. The raw dataset for each location comprises a collection of raw signal traces (*X*, *Y*, and *Z* components all included), each corresponding to a single shot labeled with receiver depth, source horizontal offset (constant for each location), and sampling rate (0.102 ms for all cases considered). All data were acquired by Fugro, who use a Fugro hydraulic underwater shearwave hammer (HUSH) box as the source, attached to the seabed frame and offset by 0.8 m.

3.3. Inversion of V_s using PH method

Analyses were run for all 110 locations; however, for the purposes of this paper, four representative cases are shown (one from each site). The maximum likelihood estimate and the 2.5$^{\text{th}}$ and 97.5$^{\text{th}}$ percentile estimates of V_s are plotted against depth for each location in Figure 2. These locations generally reflect the range of observed outcomes. Figure 2(a) is a 'reasonable' result: a relatively consistent V_s profile with few fluctuations and error bounds within a small range. Figure 2(b) demonstrates a potentially reasonable, but somewhat questionable result with some clearly unphysical outliers. Figure 2(c) and (d) show clearly unreasonable and incomprehensible profiles, respectively, with widespread *high-low fluctuations* which cannot be physical in origin. Reviewing the full range of results, the profiles for the majority of locations have characteristics similar to those of (c) and (d). A minority of profiles are as reasonable as (b) and very few as reasonable as (a).

Across the set of results, two main issues are identified: a general propensity for *high–low fluctuations* between adjacent layers, and in some cases, the presence of severe outliers. Through more detailed investigation, these two features have been found to directly stem from two separate issues which are discussed in more detail in the following sections.

3.3.1. Travel time outliers

The presence of severe outliers in V_s has been found, via inspection of intermediate results, to originate from inaccurate CC-based travel time-estimates for certain receiver pairings. This is most clearly evidenced by plotting the average travel times (i.e., the values in the $\boldsymbol{t}$ vector) in order of pairing. For N probe positions (hence $2N$ receiver depths), a logical order is: 0–1, 0–2, …, 0–(2N–1), 1–2, 1–3, …. 1–(2N–1), etc. Figure 3(a) shows

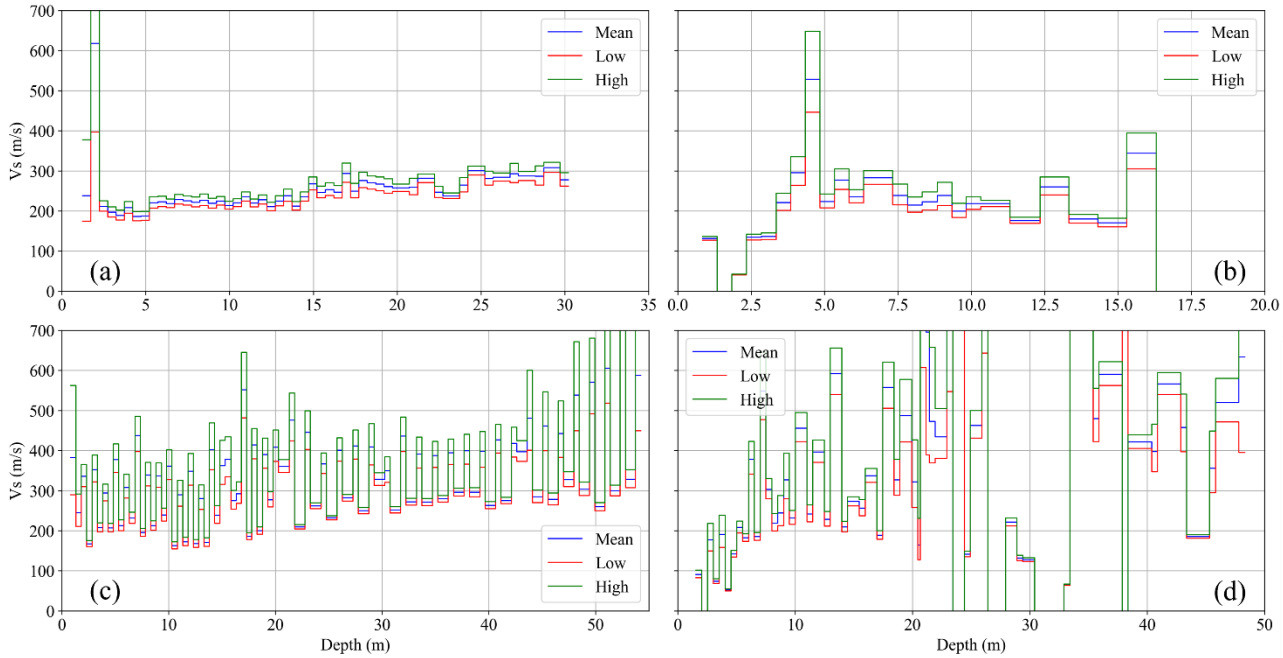

Figure 2. V_s profiles via original method for (a) HKN56-SCPT, (b) TNW005-SCPT, (c) HKW067-SCPT, and (d) IJV019-SCPT.

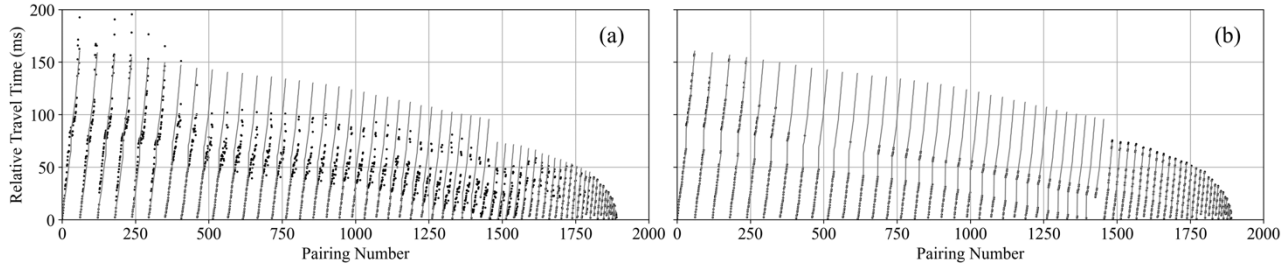

Figure 3. Mean travel time (black) derived from direct cross-correlation compared to estimates built from sums of adjacent-receiver cross-correlations (grey), (a) before and (b) after threshold-based refinement.

this plot for IJV019-SCPT. In addition, the *expected* travel time (see Section 4.1) – evaluated by accumulating the travel times calculated via CC of adjacent receivers – is plotted as a reference (grey continuous lines).

Figure 3(a) demonstrates that more distant receiver pairings tend to deviate from the *expected* travel time and are generally less reliable. This has been attributed to two main causes. Firstly, signal traces from distant receivers differ in shape more than those from nearby receivers. Evaluating the time shift between signals which appear very different from each other is much less robust. Secondly, the characteristic first peak seen in the received signal can become attenuated at large depths, meaning comparison of a shallow and deep signals may wrongly attempt to match the first peak of the shallow signal with what is actually the second peak of the deep signal, as the first is attenuated beyond detection.

3.3.2. Measurement errors

To understand the reason for the *high–low fluctuations*, which are so widely observed, it is important to consider the differences between alternating layers. For layers 0, 2, etc. (referred to as T layers), the most influential observation is a *true-interval* observation, between top receiver of a probe in one position and bottom receiver of a probe in the same position. For layers 1, 3, etc. (referred to as P layers), it is a *pseudo-interval* observation, between bottom receiver of a probe in one position, and top receiver of a probe in the next position. Considering this, the discrepancy is attributed to one or more of the following:

- A latency effect between top and bottom receiver, such that the bottom begins recording at a time Δt_{lat} later (or earlier for negative values) than the top. This would skew V_s for T layers in one direction and V_s for P layers in the other.
- A trigger delay discrepancy, such that for each P layer k, the receivers at the lower probe begin recording data $\Delta t_{trig,k}$ later than the receiver at the upper probe position. This would skew V_s for P layers.
- A depth inaccuracy such that for each P layer k, the true separation between the positions is Δd_k greater than recorded. This would skew V_s for P layers.

This hypothesis can be tested by running analyses including only data from top receivers or only data from bottom receivers, thus eliminating the effect of latency Δt_{lat} and eliminating inconsistency between *true-interval* and *pseudo-interval* observations by removing all *true-interval* observations (i.e., all included observations are subject to the same trigger delay discrepancies and depth inaccuracies). Figure 4 shows these results for location HKW067-SCPT, where the phenomenon is particularly pronounced. It is observed that the *high-low fluctuation* disappears, supporting that it is due to one or more of the aforementioned factors.

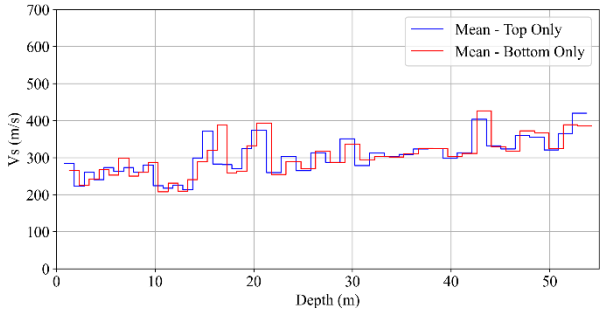

Figure 4. V_S profiles for HKW067-SCPT, considering only data from top receivers, and only data from bottom receivers.

4. Proposed formulation

4.1. Filtering of travel time outliers

It is noted that when the CC method fails to select the *true* travel time, the magnitude of the error cannot be any value but will be close to a multiple of the dominant period of the signal. Since the CC function delivers maxima only when peaks of the two signals align, incorrectly aligned signals will be some number of cycles away from the true condition, rather than some arbitrary value of time. Secondly, it is noted that in general, the variance in relative travel time for correctly evaluated pairs is much lower than the dominant period, i.e., variance of arrival time of the first peak is generally much lower than the time between the peaks themselves. Thus, a solution can be devised as follows:

- Define a threshold which sits between the magnitudes of the dominant period and the true variance of travel time. For the cases considered, the dominant frequency is generally between 35–50 Hz which corresponds to a period of 20–30 ms. The variance for most observations is of the order of 1 ms. Therefore, a 10 ms threshold is an appropriate.
- Evaluate the *expected* travel times using a traditional approach: stack all available traces for each receiver, evaluate travel times between adjacent receivers only (i.e., most reliable pairings only) using the CC approach, and cumulatively sum the relevant adjacent travel times for any given receiver pairing to obtain the reference time.
- Run the analysis as usual, but discarding any travel times which fall outside of the reference time +/- the threshold.

Note that for the cases considered in this study, the calculation of adjacent receiver travel times is further constrained to select the first peak in the correlation function as the relative travel time. This increases reliability by preventing cycle skipping, as long as the travel time is significantly less than the dominant period.

This solution results in some receiver pairings being completely discarded from the $\boldsymbol{t}$ vector. However, this does not matter as the governing Eq.4 is heavily over-specified, and as such this amounts to using fewer (but still sufficiently many) observations which are considered accurate, rather than a greater number of observations, some of which may be inaccurate.

Figure 3(b) shows the equivalent results with this filtering applied. Figure 5 shows the updated V_S profiles for IJV019-SCPT and TNW005-SCPT (noting that the other locations are less affected by this issue). The results are markedly improved, and the presence of extreme outliers is reduced. This is a crucial modification, as previously, the inaccurate observations were still treated as valid observations. This meant that if the observations were inaccurate but precise (i.e., all combinations of traces giving inaccurate but similar values), the resulting outliers in the V_S profile would exhibit low uncertainty (i.e., narrow bounds), hence the results would induce high confidence in inaccurate results.

4.2. Inclusion of measurement errors

To overcome the issue of pairing incompatibility, a refined method is proposed which attempts to include the aforementioned error terms such that the true velocity profile can be estimated in spite of errors during acquisition. Every travel time increment for a given layer m can be expressed via the following:

$$t_{m,T} = s_m G_m - \Delta t_{lat} = s_m G_m + \varepsilon_T \quad , (7)$$

$$t_{m,P} = s_m G_m + \Delta t_{lat} - \Delta t_{trig,m} + s_m \Delta d_m = s_m G_m - \varepsilon_T + \varepsilon_{P,m} \quad , (8)$$

where $t_{m,T/P}$ are the *measured* (i.e., error-prone) travel times for a signal through layer m, s_m is the slowness in layer m, and G_m is the length of the ray path through layer m. A single True (T) error term ε_T describes the latency between top and bottom receivers, and if there are N receiver positions, N–1 Pseudo (P) error terms $\varepsilon_{P,m}$ describe the lumped pseudo-time errors due to trigger delay discrepancy and/or depth inaccuracy. All travel times are expressed as some combination of the above layer-based time increments. In other words, $\mathbf{G}$ is built from various combinations of these expressions. Introduction of the error terms allows for the high-low values of V_S to be aligned. However, it is complex to evaluate them as the problem is now underspecified. Previously there were as many fundamental observations as unknowns ($2N$–1 layer-based time increments and $2N$–1 unknown slownesses). Now there are also N–1 P error and 1 T error unknowns. Therefore, assumptions must be made in order evaluate these additional unknowns.

Before defining the mathematical formulation, it is useful to consider qualitatively what these additional parameters achieve. The P error parameters $\varepsilon_{P,m}$ exist for every P layer and therefore in theory allow the P slownesses to be brought in line with the T slownesses. However, since the T error parameter ε_T acts against them (by changing the T slownesses), there are infinite combinations of ε_T and the set of $\varepsilon_{P,m}$. Adjusting ε_T will allow the aligned profile to be shifted as a whole, thus bringing it closer to either the original P slownesses or the original T slownesses. Without prior knowledge on the magnitude of these errors, these two possibilities are equally likely. With prior knowledge on the likelihood of these errors, the more likely possibility can be realised.

Let the fundamental Eq.4 be modified such that:

$$\boldsymbol{t} = \mathbf{G}\boldsymbol{s} + \boldsymbol{\Sigma}\boldsymbol{\varepsilon} \quad , (9)$$

$$\boldsymbol{\varepsilon} = \left[\varepsilon_{P,0} \;\; \varepsilon_{P,1} \;\; \cdots \;\; \varepsilon_{P,N-2} \;\; \varepsilon_T\right]^{\mathrm{T}} \quad , (10)$$

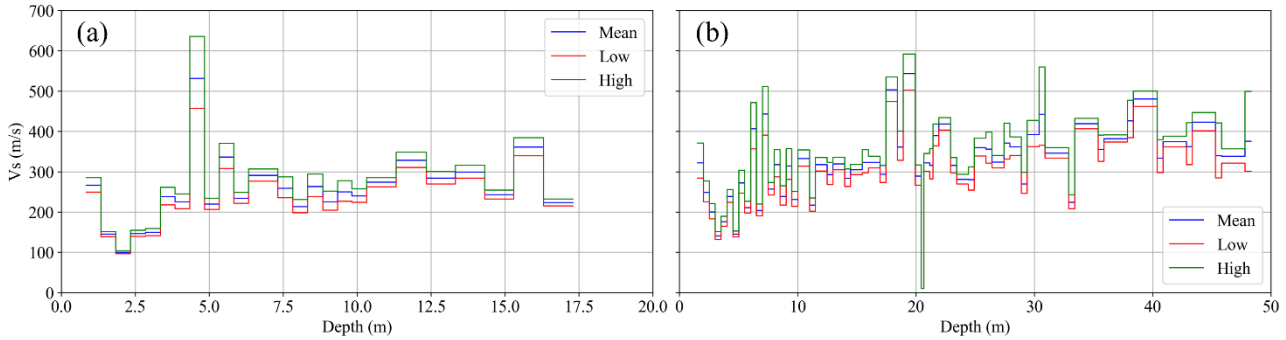

Figure 5. Vs profiles via refined method with threshold-based observation for (a) TNW005-SCPT and (b) IJV019-SCPT.

where $\boldsymbol{\Sigma}$ contains the coefficients of each error term to be added. For each travel time observation (i.e., row), coefficients are 0 or 1 for each $\varepsilon_{P,m}$ (i.e., column) depending on which P layers are encompassed, and the coefficient of ε_T is –1, 0, or 1, depending on whether the two receiver positions are bottom–top, top–top/bottom–bottom, or top–bottom, respectively.

Now let N–1 constraints, related to compatibility of T and P slownesses, be defined. Each P slowness should be equal to the average of the adjacent T slownesses ($2s_{i(P)} - s_{i-1(T)} - s_{i+1(T)} = 0$), allowing for a tolerable variance. This variance should be a measure of the local spatial variability of slowness. Here, it is estimated as follows:

- Calculate all approximate T slownesses as $s_k = (T_{k+1} - T_k)/(d_{k+1} - d_k)$ for k = 0, 2, 4, …, N–2, where the travel times $T_{k+1} - T_k$ are calculated as for the expected travel times in Section 4.1.
- Calculate variances $\sigma^2{}_k = \mathrm{var}(s_k, s_{k+2})$ for k = 0, 2, 4, …, N–4 .
- Estimate representative variance as the average of all variances: $\overline{\sigma^2} = \mathrm{average}(\sigma^2{}_k)$.

The set of constraints can be then expressed as follows:

$$\mathbf{0} = \mathbf{B}\boldsymbol{s} \quad . (11)$$

Each row of the **B** matrix corresponds to a P layer, and contains the terms -1, 2, -1 for the corresponding layer and its adjacent T layers. The 0 values are uncertain and associated with the covariance matrix $\mathbf{C_b} = 4\,\overline{\sigma^2}\mathbf{I}$. Finally, a new governing equation can be formed:

$$\boldsymbol{t}^{\mathrm{X}} = [\boldsymbol{t} \quad \mathbf{0}]^{\mathrm{T}} = \mathbf{G}^{\mathrm{X}}\boldsymbol{s}^{\mathrm{X}} = \begin{bmatrix} \boldsymbol{G} & \boldsymbol{\Sigma} \\ \boldsymbol{B} & \mathbf{0} \end{bmatrix} [\boldsymbol{s} \quad \boldsymbol{\varepsilon}]^{\mathrm{T}} \quad , (12)$$

$$\mathbf{C_d}^{\mathrm{X}} = \begin{bmatrix} \mathbf{C_d} & \mathbf{0} \\ \mathbf{0} & \mathbf{C_b} \end{bmatrix} \quad . (13)$$

Given that this new expression follows the same algebraic form as the original formulation, the same inversion method can be followed to derive the most likely slowness vector $\boldsymbol{s}$, and now additionally the error vector $\boldsymbol{\varepsilon}$, via one combined vector $\boldsymbol{s}^{\mathrm{x}}$. However, it must be stressed that given the under-specification of the $\mathbf{G}^{\mathrm{x}}$ matrix, the solution will only exist if a prior is specified on one or more of the error terms.

This new framework, for given prior knowledge on the error terms, should allow for a smooth profile to be evaluated which accounts for the pairing incompatibility as additional uncertainty and/or a relative shift towards the original T or P profile. Prior knowledge is specified via normal distributions for ε_T and ε_P, with zero mean and a standard deviation related to the expected magnitude of the errors. These values are included in Eq.5 and Eq.6 via $\boldsymbol{s}^{\mathrm{x}}_{\mathbf{p}}$ and $\mathbf{C}^{\mathrm{x}}_{\mathbf{p}}$, noting that all entries related to slowness (s) rather than error (ε) are set to zero. The expected magnitude of the errors has been estimated as follows:

The timing errors Δt_{lat} and Δt_{trig} are assumed to be of the order of the sampling rate (in this case, 0.10 ms), based on the implication by Parasie et al. (2022) that timing errors reduce as the sampling rate decreases. For the depth error, a CPT with application Class 2 (ISO 22476-1:2022) should exhibit <0.2 m error at 10 m penetration. Assuming this is a normally distributed error, which is an accumulation of normally distributed errors associated with each push, the equivalent error for each push is approximately <0.2 m/$\sqrt{N_{pushes}}$. For this dataset, the push length is generally 1 m, hence a representative magnitude for Δd is estimated as 0.063 m. For a (conservative) V_s of 200 m/s, the subsequent travel time error would be 0.32 ms. Based on the above, standard deviations of 0.1 ms and 0.4 ms are recommended for ε_T and ε_P, respectively.

4.3. Results and discussion

Figure 6 presents the results from the new method under the base condition of prior knowledge. The results show the derived estimates of $\boldsymbol{s}$, as previously, and now also show the derived maximum likelihood error terms ε_T and ε_P which are available through the estimated $\boldsymbol{s}^{\mathrm{x}}$.

In all cases, a smoother, coherent profile is derived which allows for genuine interpretability when compared with the original profiles hindered by the alternating values. The base priors are sufficient to account for and rectify even the most severe errors, hence these are justified as preliminary conditions for any given location.

However, weaker priors in general lead to larger uncertainty bounds. This reflects the fact that there are many combinations of ε_T and ε_P which are not penalised too heavily by the prior variance, i.e., both can increase in opposite directions without too much penalty, widening the bounds of possible V_s. Therefore, in some cases where the actual magnitude of the errors is much smaller than the priors, the uncertainty bounds will be unnecessarily large. In some extreme cases (HKW067-SCPT and IJV019-SCPT), it is likely that the errors are in the order of the base case, hence such priors are realistic and the resulting uncertainty bounds are valid. In others (HKN56-SCPT), the error terms are likely to be of much smaller magnitude. Their expected magnitude can be re-assessed through the most likely error plots in Figure 6. These error plots are highly informative in

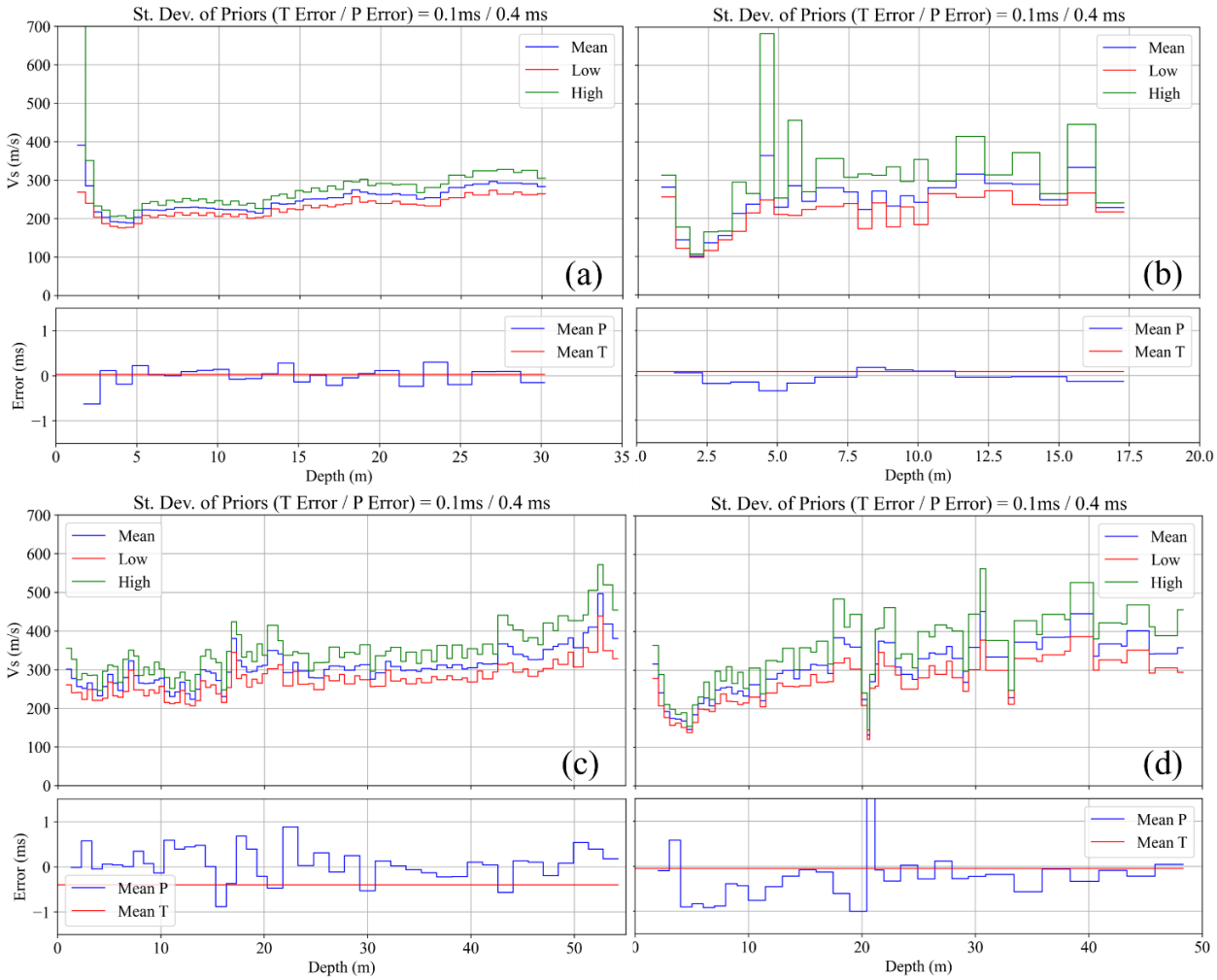

Figure 6. V_s profiles and corresponding most likely error terms ε via new method for (a) HKN56-SCPT, (b) TNW005-SCPT, (c) HKW067-SCPT, and (d) IJV019-SCPT.

terms of assessing the overall quality of the data. If they are high, it suggests that significant measurement errors are embedded in the data, i.e., the test is of low quality: either there were significant timing errors or there was significant depth inaccuracy. Such reliability assessment is not available when using traditional methods.

As a result, should uncertainty bounds need to be reduced, a second pass of the analysis for any given location can be run, with reduced-variance priors informed by the maximum likelihood error terms derived through the initial analysis. This has been run for HKN56-SCPT, displayed in Figure 7. It is observed that the most likely V_s profile remains relatively unchanged, but the uncertainty bounds are reduced. Thus, for any given location, this optimised profile represents the minimal level of uncertainty required to be able to generate a smooth profile devoid of erroneous, alternating high-low values. The implication of this is that for low quality tests with high error terms, the final uncertainty will be high, whereas for high quality tests with low error terms, the final uncertainty will be low.

Alternatively, the T or P error terms can initially be specified with low variance if measurements are assumed to be accurate. For example, it is often perceived that *true-interval* measurements are significantly more reliable than *pseudo-interval*. From Figure 6, this is seen to be a valid assumption for HKN56-SCPT and IJV019-SCPT, but is more questionable for HKW067-SCPT. To examine the effect of such a specification, Figure 8 demonstrates the results for HKW067-SCPT with a reduced prior standard deviation of 0.01 ms for T error.

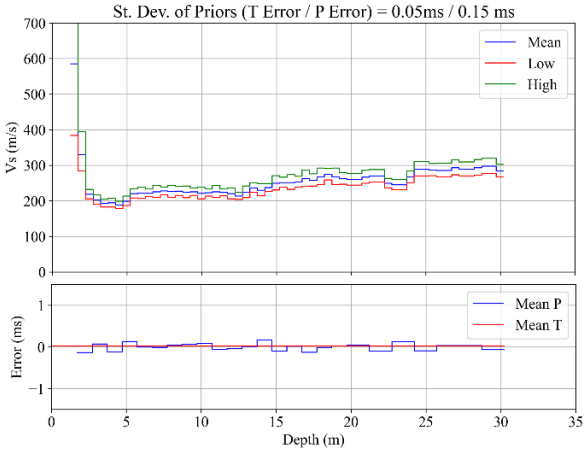

Figure 7. V_s profile and most likely error terms ε with optimised priors for HKN56-SCPT (left).

Firstly, the profile is seen to be shifted higher than the first-pass results, reflecting the increased confidence in the T values, which were originally much higher than the P values. Secondly, the P and T values are not able to be

aligned by ε_P alone, suggesting that the P errors would have to be even larger than the derived values seen in the Figure (which are limited by the 0.4 ms prior). From the error plot, these derived values are all now centered around a value of 0.6 ms. For a purely depth-based error (i.e., no trigger time discrepancy) and a representative V_s of 350 m/s (as observed), 0.6 ms would correspond to a systematic depth error Δd of 0.21 m for every 1 m push throughout the full profile. This seems unreasonable (particularly since the errors would likely have to be even higher, as discussed), which suggests that for this location, assuming the T error to be zero is perhaps overly naïve. For cases where latency exists/T error is non-zero (which the above demonstrates are likely to exist, albeit not unanimously), this error would heavily influence the results from a traditional interval method interpretation (which only assesses T layers), all while remaining completely undetected. The recommended procedure, therefore, is to: (i) apply the adapted method initially with the recommended priors, such that the magnitude of errors can be evaluated and reflected in the V_s uncertainty bounds, and (ii) where the operator has confidence that measurement errors are small, they may induce stronger priors on certain errors informed by the derived maximum likelihood errors, and/or their own judgment.

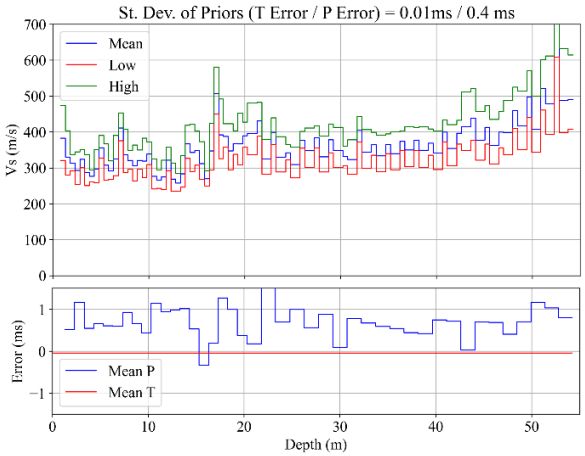

Figure 8. V_s profile and most likely error terms with near-zero T-error prior for HKW067-SCPT,

5. Conclusions

A modified method for Bayesian interpretation of SCPT data has been proposed, based on the work of Pidlisecky and Haines (2011). The first modification is a procedure for identification and removal of inaccurate travel time estimates, leading to more reliable and accurate V_s profiles as outliers are avoided. The second modification is a reformulation of the fundamental model equation to incorporate timing and/or depth errors, which increases robustness of the method against real, often imperfect datasets. Analysis across over 100 locations has shown that such errors are frequent and influence derived V_s values, even though traditional methods would not detect them. The new model in its base form delivers a smooth V_s profile with uncertainty bounds that account for measurement errors in the data. Additionally, the formulation allows for an engineer to reduce the prior likelihood of certain errors should they feel confident to do so, reducing the uncertainty of the profile.

This method provides valuable information on the reliability of the data by estimating measurement errors directly. Traditional methods ignore such errors, hence can sometimes deliver inaccurate results. Therefore, this method is recommended to ensure results can be relied upon. At the very least, a *true* and a *pseudo-interval* analysis should both be performed. Their compatibility will indicate the significance of timing and/or depth errors – a key consideration when assessing reliability.

Acknowledgements

The authors are grateful for the support of Scottish Power Renewables, Geowynd, and the University of Glasgow. RVO own, publish, and license the data used in this study under a Creative Commons 4.0 CC BY SA license.

References

Baziw, E. 1993. “Digital Filtering Techniques for Interpreting Seismic Cone Data.” J Geotech Eng 119 (6): 998–1018.

Baziw, E., G. Verbeek. 2016. “Frequency Spectrum ‘Bell-Curve’ Fitting as a Component of SCPT Interval Velocity Accuracy Assessment.” In Proc 5th Intl Conf Geotechnical and Geophysical Site Characterization (ISC5): 1431–1435.

Buckley, R. M., Y. Chen, B. B. Sheil, D. Xu, J. P. Doherty, and M. F. Randolph. 2023. “Bayesian Optimisation for CPT-Based Prediction of Impact Pile Driveability.” J Geotech and Geoenv Eng - ASCE 49 (11).

Campanella, R. G., P. K. Robertson, and D. Gillespie. 1986. “A Seismic Cone Penetrometer for Offshore Applications.” In Oceanology, 479–86. Springer.

ISO 22476-1:2022. 2022. “Geotechnical Investigation and Testing - Field Testing - Part 1: Electrical Cone and Piezocone Penetration Test.”

Lo, M. K., X. Wei, S. C. Chian, and T. Ku. 2021. “Bayesian Network Prediction of Stiffness and Shear Strength of Sand.” J Geotech and Geoenv Eng 147 (5): 4021020.

Malinverno, A., and V. A. Briggs. 2004. “Expanded Uncertainty Quantification in Inverse Problems: Hierarchical Bayes and Empirical Bayes.” Geophysics 69 (4): 1005–16.

Parasie, N., T. Franken, and J. Peuchen. 2022. “Assessment of Seismic Cone Penetration Testing for Small Strain Shear Modulus.” In Cone Penetration Testing 2022, 203–8. CRC Press.

Peuchen, J., and R. Wemmenhove. 2020. “Depth Accuracy of Data Points in Marine Soil Investigation.” In Proc 4th Intl Symp on Frontiers in Offshore Geotechnics (ISFOG 2020): 1036–45.

Pidlisecky, A., and S. S. Haines. 2011. “A Bayesian Approach for Determining Velocity and Uncertainty Estimates from Seismic Cone Penetrometer Testing or Vertical Seismic Profiling Data.” Canadian Geotech Journal 48 (7): 1061–69.

Stolte, A. C., and B. R. Cox. 2019. “Towards Consideration of Epistemic Uncertainty in Shear Wave Velocity Measurements Obtained via SCPT.” Canadian Geotechnical Journal 57 (1): 48–60.

Stuyts, B., C. S. Jurado, D. G. Bautista, and A. Kheffache. 2022. “Bayesian Estimation of Small-Strain Shear Modulus from Offshore CPT Tests in the North Sea.” In Cone Penetration Testing 2022, 722–27. CRC Press.

Tarantola, A. 2005. Inverse Problem Theory and Methods for Model Parameter Estimation. SIAM.

Vinck, K. 2021. “Advanced Geotechnical Characterisation to Support Driven Pile Design at Chalk Sites.”

Wang, H., S. Wu, X. Qi, and J. Chu. 2021. “Modified Refracted Ray Path Method for Determination of Shear Wave Velocity Profiles Using Seismic Cone.” Engineering Geology 293: 106330.